



ENHANCED FORECASTING OF BIOMASS-TOXICITY-WATER MODELS USING NUMERICAL SIMULATIONS

MUDASSAR ABBAS^{✉*1}, FRANCESCO GIANNINO^{✉2},
ANNALISA IUORIO^{✉3} AND FRANCESCO CALABRÒ^{✉1}

¹Department of Mathematics and Applications “Renato Caccioppoli”,
University of Naples Federico II, Via Cintia, Monte S. Angelo, Naples, I-80126, Italy

²Department of Agricultural Sciences, University of Naples Federico II,
Via Università, Portici(NA), I - 80055, Italy

³Department of Engineering, Parthenope University of Naples,
Centro Direzionale - Isola C4, Naples, I - 80143, Italy

ABSTRACT. Numerical techniques are essential tools to solve reaction-diffusion models in ecology, addressing the intrinsic complexity arising from nonlinear and coupled systems. Advanced numerical methods provide efficient spatial and temporal resolution in order to predict the emergence of complex patterns, such as the ones arising in vegetation. The emergence of vegetation patterns is significantly influenced by plant-soil feedback, which alters soil properties, shapes nutrient availability, influences plant interactions, and develops mutualistic relationships with soil microbes. Understanding these feedback processes is essential to manage and conserve ecosystems, predict responses to environmental change, and implement appropriate land management strategies. The formation of vegetation patterns has been the focus of significant study and debate over the years and has been linked to two main mechanisms: the depletion of water in the center of vegetation patches and the production of toxicity by litter decomposition in soil. In this study, we investigate the role of water depletion and autotoxicity in the formation of spatial vegetation patterns. We propose and compare various reaction-diffusion PDE models that describe the dynamics of plant biomass under water scarcity and the presence of toxicity caused by litter decomposition. We incorporate logistic and exponential growth functions to capture different growth mechanisms, along with mortality and inhibition terms to simulate the components' individual death rates and inhibitory effects. This leads us to six alternative reaction-diffusion PDE models, which we solve using suitable numerical techniques.

1. Introduction. Plant ecologists have been fascinated by the complexities of vegetation dynamics for a long time [12, 13, 54]. The ecological importance of regular vegetation patterns in arid and semi-arid landscapes indicates the need for further investigation to enable efficient management and conservation of these ecosystems. Regular vegetation patterns arise and are maintained by a complex interplay of components, including self-organizing processes driven by feedback mechanisms between environmental variables and plants [36, 45]. These patterns affect water flow, the

2020 *Mathematics Subject Classification.* Primary: 86A08; Secondary: 65P40, 35B36, 65M06.

Key words and phrases. Mathematical models, vegetation patterns, plant-soil feedback, litter decomposition, forecasting via numerical simulations.

*Corresponding author: Mudassar Abbas.

nutrient cycle, habitat availability, and ultimately the distribution of plant species [28, 34]. To sustainably manage land, an understanding of the mechanisms underlying regular vegetation patterns and the ecological consequences of these patterns is required [45]. Regular vegetation patterns are essential to the resilience, biodiversity, and proper operation of ecosystems. Understanding these patterns is crucial for effective land management and conservation efforts in fragile areas [9, 22].

Activator-inhibitor reaction-diffusion models have been effectively utilized to study various real-life problems [23, 30]. A variety of systems exhibiting patterned dynamics, including vegetation, are studied using PDE models based on activator-inhibitor interactions [11, 21, 35]. In these models, the inhibitor limits the activator's production, whereas the activator stimulates its own. Diffusion of both the activator and inhibitor plays a key role in the dynamics of these models, which in fact are based on reaction-diffusion equations. It was Alan Turing who first observed the patterns that arise in these models in 1952; he proposed that the destabilization of a stable, spatially uniform steady state through the coupling of diffusion and kinetics leads to pattern formation [48]. In particular, Turing's theory was effectively used to provide a suitable explanation of the spatially periodic structures of vegetation biomass that emerge over flat terrains as well as along slopes [6, 10, 15, 19, 20, 24, 27, 42, 44, 52]. In the first case, the resulting patterns referred to labyrinths, hexagons, gaps, and spots [14, 16, 17, 18, 25, 30, 36, 38, 40, 47, 53] while in the latter case, these formations are called bands, tiger bushes, or stripes [10, 15, 27, 39, 41, 43, 46, 51, 55].

One of the main ecological hypotheses relates the emergence of vegetation patterns to the availability of water and was described by coupled partial differential equations (PDEs) governing plant biomass and water dynamics [24, 31, 32, 33, 36, 50, 53]. However, the existence of patterns in humid environments could not be explained by only considering water availability [37]. An additional relevant ecological mechanism that should be taken into account is thus given by plant-soil negative feedback; this involves soilborne pathogens which can reduce the growth, reproduction, and survival of plants [2, 7, 8], and autotoxic compounds produced from litter decomposition [4, 29]. The toxic environment prevents seed germination and growth [5]. PDE models combining the dynamics of biomass, toxicity, and soil water can replicate vegetation patterns even in situations where water is not a limiting factor [26].

In our previous work [1], we used the reaction-diffusion framework to study the formation of vegetation patterns on flat terrains, by considering plant biomass as the activator and soil toxicity as the inhibitor. In this context, high biomass levels promote the production of toxins, which in turn inhibit plant growth. This feedback loop can lead to the formation of stable vegetation patterns, such as stripes, spots, and bands but is unable to support the emergence of Turing patterns. In this work, we include water as a third state variable playing the role of the substrate. We then proposed several reaction-diffusion models by considering different types of growth, mortality, and inhibition functions. This approach leads to six PDE models, allowing for a comprehensive exploration of individual and combined effects of water and autotoxicity on the biomass spatial distribution.

The rest of this paper is structured as follows. In Section 2 we introduce the general framework used for the PDE models analysed in this work based on the dynamics of an activator, a substrate, and an inhibitor (respectively representing biomass, water, and autotoxicity). Taking into account different types of growth,

mortality, and inhibition functions leads to six PDE models, which are introduced in Section 3. The numerical scheme and the corresponding results of the simulations of these six models are discussed in Section 4. Finally, the implications of our findings are discussed in Section 5.

2. The activator-substrate-inhibitor formulation. In this study, we expand our work from [1] where we examined the role of negative plant-soil feedback to the dynamics of plant biomass. Specifically, in [1] presented the comparison of different activator-inhibitor reaction-diffusion PDE models to investigate the effect of toxicity produced by litter decomposition on plant biomass. Six models were introduced by taking biomass as an activator and toxicity as an inhibitor to study the corresponding dynamics. In this work, we integrated the activator-inhibitor models in [1] by adding a substrate component. A substrate is a material or resource consumed in the reaction (e.g., water, ammonium, sulfate). Here we focus on two growth functions in order to capture the main growth mechanisms observed in nature: logistic and exponential. The logistic growth incorporates inhibitory effects and, by including the carrying capacity related to the environment, takes into account the influence of potentially limiting factors. On the other hand, the exponential function mimics unrestricted growth under ideal conditions. Moreover, we distinguish different strategies for the inhibitor to limit the activator's dynamics; in particular, we consider growth inhibition, extra mortality, and a combination of both effects.

The general configuration of the mathematical models defining the dynamics of three components - the activator (A), the inhibitor (I), and the substrate (S) - thus takes the form

$$\begin{aligned}\frac{\partial A}{\partial t} &= \Phi_A(A, S, I) + D_A \nabla^2 A, \\ \frac{\partial S}{\partial t} &= \Phi_S(A, S, I) + D_S \nabla^2 S, \\ \frac{\partial I}{\partial t} &= \Phi_I(A, S, I) + D_I \nabla^2 I.\end{aligned}\tag{1}$$

The terms modeling different growth, inhibition, and mortality processes for the activator, substrate, and inhibitor, respectively, are represented by the functions Φ_A , Φ_S , and Φ_I . The diffusion of the activator, substrate, and inhibitor is modeled by the Laplacian operator ∇^2 (which only acts on the spatial domain) with corresponding diffusion coefficients D_A , D_S , and D_I . In the context of vegetation dynamics, we consider the dynamic interactions of plant biomass as the activator, water as the substrate, and toxic compounds as the inhibitor. These are analyzed in terms of densities, represented by the variables B , W , and T , respectively.

TABLE 1. Notation for the PDE models in Sec. 3.

		Inhibitor type		
		Inhibition	Extra Mortality	Inhibition and Extra mortality
Activator type	Exponential	BETIW	BETMW	BETIMW
	Logistic	BLTIW	BLTMW	BLTIMW

3. The PDE models for vegetation dynamics. The proposed models consist of three nonlinear coupled partial differential equations. In particular, the notation that we outlined in Table 1 and the reaction terms of the proposed models are summarised in Table 2.

TABLE 2. Activator-Substrate-Inhibitor models as in (1) in the case of biomass (B), water (W) and toxicity (T).

		Toxicity		
		Inhibition	Extra Mortality	Inhibition and Extra Mortality
Biomass	Exponential	$\Phi_A = gB^2(1 - T)W - dB$ $\Phi_S = p - rB^2W - lW$ $\Phi_I = cgB^2(1 - T)W - kT$	$\Phi_A = gB^2W - dB - sBT$ $\Phi_S = p - rB^2W - lW$ $\Phi_I = c(dB + sBT) - kT$	$\Phi_A = gB^2(1 - T)W - dB - sBT$ $\Phi_S = p - rB^2W - lW$ $\Phi_I = c_1gB^2(1 - T)W + c_2(dB + sBT) - kT$
	Logistic	$\Phi_A = gB(1 - \frac{B}{B_m}) \times (1 - T)W - dB$ $\Phi_S = p - rB^2W - lW$ $\Phi_I = cgB(1 - \frac{B}{B_m}) \times (1 - T)W - kT$	$\Phi_A = gB(1 - \frac{B}{B_m})W - dB - sBT$ $\Phi_S = p - rB^2W - lW$ $\Phi_I = c(dB + sBT) - kT$	$\Phi_A = gB(1 - \frac{B}{B_m})(1 - T) \times W - dB - sBT$ $\Phi_S = p - rB^2W - lW$ $\Phi_I = c_1gB(1 - \frac{B}{B_m}) \times (1 - T)W + c_2(dB + sBT) - kT$

These models combine extra mortality and inhibition terms with logistic and exponential growth functions to investigate the impact of various factors on the dynamics. The impact of different variables on the dynamics of toxicity, water, and biomass was specifically examined using these six different models. This approach allows for a nuanced exploration of how growth functions, mortality terms, and inhibition processes shape the overall behavior and distribution of the state variables. The study aims to contribute a comprehensive understanding of the complex dynamics governing the interactions of biomass, water, and toxicity within ecological systems, offering valuable insights into the impact of different regulatory factors on vegetation patterns. In the next subsections, we will discuss the models to fix notations and refer to the examined cases. Some of the parameters will be fixed in all the considered cases; these are summarized in Table 3. A complete summary of the parameter values (and their description) is provided in Marasco et al. [26].

In all these models we present below, we consider the following common processes:

- seeds dispersal, modelled as biomass diffusion via the term $D_B \nabla^2 B$;
- water input by means of rainfall, modelled by the precipitation rate p ;
- water evaporation, described as $-lW$;
- water uptake by plants' roots, modelled as rB^2W ;
- water diffusion, described by the term $D_W \nabla^2 W$;
- toxicity intrinsic decay, modelled by the term $-kT$;
- toxicity diffusion, described by the term $D_T \nabla^2 T$.

TABLE 3. Table of Parameters.

Parameter	Description	Units	Values
g	Growth rate of B	$month^{-1}$	0.002
B_m	Carrying capacity for B	$kg\ cm^2$	1
d	Death rate of B	day^{-1}	0.01
s	Plant sensitivity to T	$cm^2kg\ month^{-1}$	0.2
D_B	Diffusion coefficient for B	cm^2month^{-1}	0.01
p	rainfall	$kg\ day^{-1}m^{-2}$	0.7-2.0
r	water uptake due to biomass	$m^4day^{-1}kg^{-2}$	0.35
l	water loss due to evaporation	day^{-1}	0.01
D_W	water diffusion coefficient	m^2day^{-1}	0.8
D_T	Diffusion coefficient for T	cm^2month^{-1}	0.5
k	Decay rate of T	$month^{-1}$	0.001-0.1
c_1	Growth rate of T due to dead biomass	–	0.05
c_2	Growth rate of T due to growth of biomass	–	0.05

We highlight that the modeling choice for the relation between biomass and water both in biomass growth and water uptake takes the form B^2W due to biomass-water feedback, as clearly explained in detail in [3].

3.1. BETIW model. In the BETIW model, the function used to model the biomass growth is exponential, proportional to water availability by a factor g and inhibited by the presence of toxicity. Toxic compounds increase proportionally to the growth of biomass via a factor c .

According to the above description, the model equations are

$$\begin{aligned}\frac{\partial B}{\partial t} &= gB^2(1-T)W - dB + D_B\nabla^2 B \\ \frac{\partial W}{\partial t} &= p - rB^2W - lW + D_W\nabla^2 W \\ \frac{\partial T}{\partial t} &= cgB^2(1-T)W - kT + D_T\nabla^2 T.\end{aligned}\tag{2}$$

3.2. BETMW model. In the BETMW model, we again assume biomass growth to be exponential and proportional to the water density with a coefficient g . Moreover, an extra mortality effect due to the presence of toxicity is described by the

term $-sBT$, where s represents the species' sensitivity. Toxic compounds are again produced by a fraction of dead biomass c .

According to the above description, the model equations are

$$\begin{aligned} \frac{\partial B}{\partial t} &= gB^2W - dB - sBT + D_B \nabla^2 B \\ \frac{\partial W}{\partial t} &= p - rB^2W - lW + D_W \nabla^2 W \\ \frac{\partial T}{\partial t} &= c(dB + sBT) - kT + D_T \nabla^2 T \end{aligned} \tag{3}$$

3.3. BETIMW model. In the BETIMW model, the two previous modelling frameworks presented in Sec. 3.1-3.2 are combined by considering both growth inhibition and extra mortality in the biomass equation, respectively represented by the terms $gB^2(1 - T)W$ and $-sBT$. In this case, toxic compounds increase proportionally to the growth of biomass by a factor c_1 and also proportionally to the dead biomass by a factor c_2 .

According to the above description, the model equations are

$$\begin{aligned} \frac{\partial B}{\partial t} &= gB^2(1 - T)W - dB - sBT + D_B \nabla^2 B \\ \frac{\partial W}{\partial t} &= p - rB^2W - lW + D_W \nabla^2 W \\ \frac{\partial T}{\partial t} &= c_1gB^2(1 - T)W + c_2(dB + sBT) - kT + D_T \nabla^2 T. \end{aligned} \tag{4}$$

3.4. BLTIW model. In the BLTIW model, the function used to model the biomass growth is logistic with carrying capacity B_m , proportional to water availability by a factor g and inhibited by the presence of toxicity. Toxic compounds increase proportionally to the growth of biomass by a factor c .

According to the above description, the model equations are

$$\begin{aligned} \frac{\partial B}{\partial t} &= gB \left(1 - \frac{B}{B_m} \right) (1 - T)W - dB + D_B \nabla^2 B \\ \frac{\partial W}{\partial t} &= p - rB^2W - lW + D_W \nabla^2 W \\ \frac{\partial T}{\partial t} &= cgB \left(1 - \frac{B}{B_m} \right) (1 - T)W - kT + D_T \nabla^2 T \end{aligned} \tag{5}$$

3.5. BLTMW model. In the BLTMW model, we again assume biomass growth to be logistic with carrying capacity B_m and proportional to the water density via a coefficient g . Moreover, an extra mortality effect due to the presence of toxicity is described by the term $-sBT$, where s represents the species' sensitivity to toxicity. Toxic compounds are again produced by a fraction of dead biomass c .

According to the above description, the model equations are

$$\begin{aligned}\frac{\partial B}{\partial t} &= gB \left(1 - \frac{B}{B_m}\right) W - dB - sBT + D_B \nabla^2 B \\ \frac{\partial W}{\partial t} &= p - rB^2W - lW + D_W \nabla^2 W \\ \frac{\partial T}{\partial t} &= c(dB + sBT) - kT + D_T \nabla^2 T.\end{aligned}\tag{6}$$

3.6. BLTIMW model. In the BLTIMW model, the two previous modelling frameworks presented in Sec. 3.4-3.5 are combined by considering both growth inhibition and extra mortality in the biomass equation, respectively represented by the terms $gB \left(1 - \frac{B}{B_m}\right) (1 - T)W$ and $-sBT$. Toxic compounds increase proportionally to the growth of biomass by a factor c_1 and to the dead biomass by a factor c_2 .

According to the above description, the model equations are

$$\begin{aligned}\frac{\partial B}{\partial t} &= gB \left(1 - \frac{B}{B_m}\right) (1 - T)W - dB - sBT + D_B \nabla^2 B \\ \frac{\partial W}{\partial t} &= p - rB^2W - lW + D_W \nabla^2 W \\ \frac{\partial T}{\partial t} &= c_1 gB \left(1 - \frac{B}{B_m}\right) (1 - T)W + c_2 (dB + sBT) - kT + D_T \nabla^2 T.\end{aligned}\tag{7}$$

4. Forecasting: Numerical simulations. In this section, we performed the numerical simulations of the models given in Sec. 3, with the goal of examining the spatial dynamics of the systems in various ecosystems, represented by different precipitation rates p . Here, we focus our attention on the one-dimensional case as this allows a clear comparison with the stability results shown in section A. Additional simulations carried out on a two-dimensional domain are discussed in Sec. 5. All our models of type (1) are defined on the bounded domain $\Omega = \{0 \leq x \leq L\}$ and are subject to the boundary and initial conditions

$$\begin{cases} \frac{\partial B}{\partial x} = 0, & x \in \partial\Omega, & t \geq 0, \\ \frac{\partial W}{\partial x} = 0, & x \in \partial\Omega, & t \geq 0, \\ \frac{\partial T}{\partial x} = 0, & x \in \partial\Omega, & t \geq 0, \end{cases}\tag{8}$$

and

$$\begin{cases} B(x, 0) = \mathcal{A} \exp\left(-\frac{(x-x_0)^2}{2\sigma^2}\right), & \text{for all } x, \\ W(x, 0) = 0, \\ T(x, 0) = T_0, \end{cases}\tag{9}$$

where \mathcal{A} is the height of the Gaussian pulse, $x_0 = L/2$ is its center and $\sigma = 3$ is its width. All numerical simulations are carried out with $L = 30$. We use zero flux Neumann boundary conditions in our models to mimick a limited spatial area with no exchange across the boundaries in order to focus on the internal dynamics of the system.

In the next section, we first provide a detailed description of the numerical scheme used in our simulations and then present results of the evolution of biomass for the different models introduced in Sec. 3. For each model, we fix three different initial conditions by varying the value of \mathcal{A} in Eq. (9) and then display three panels corresponding to the time evolution of the biomass dynamics for different values of the precipitation rate p (according to Table 2). In all cases, we will consider that a single figure (with two or three panels) is presented for the same initial condition, so that the figures in the same section differ for the choice of \mathcal{A} , see equation (9). The panels in the figures differ for the choice of the precipitation rate p , see Table 2.

4.1. Numerical scheme. We treat the time derivatives in our models in Sec. 3 for the one-dimensional case using the Implicit Euler method because of its unconditional stability. With the use of the Implicit Euler Method, we discretize the spatial and temporal domain in n and k steps, respectively, with a grid spacing of dx and dt .

After reorganizing the terms, the system becomes:

$$MU = \mathcal{N}(U) \tag{10}$$

where \mathcal{N} represents the nonlinear terms, U is used for state variables (A , S and I), and M is the matrix involving the coefficients of linear terms.

1. To solve the above system of nonlinear equations, we choose a fixed point iteration technique for the numerical evolution of $U(i, j)$, i.e, $U(i, j) \approx U(x_i, t_j)$, where $x_i = x_0 + idx$ and $t_j = t_0 + jdt$, where i is the index of the grid points in space and j is the index of the time steps.
2. Let $U^k(i, j)$ be the value of $U(i, j)$ at the k^{th} iteration, we find the solution at the current time step using the solution at the previous time step $U(i, j - 1) = U^0(i, j)$ as an initial guess.
3. Using the following formula, we determine the new value of $U^{k+1}(i, j)$ at each iteration:

$$MU^{k+1} = \mathcal{N}(U^k) \tag{11}$$

and the iteration is carried out until the error between iterations is less than a certain tolerance.

Despite all these precautions, we still observe occasional instances of instability in the numerical scheme. In our view, this arises from the incompatibility between the boundary conditions and the internal operator. Improved results might have been achieved with a different ratio between the spatial and temporal discretization parameters. However, we chose not to include results using alternative ratios, as our aim is to highlight that such instabilities require a different numerical approach. In future research, we plan to develop a more robust scheme to address these challenges.

The simulations are performed in MATLAB that has been used on a laptop PC with Intel i7 core.

4.2. Results for BETIW model. The obtained results in the case of BETIW model (2) (Figures 1-3) indicate that the model can exhibit patterns or constant steady-state behavior depending both on the precipitation rate and on the initial

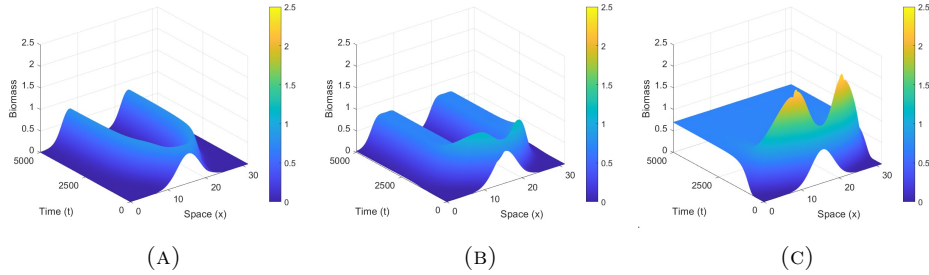


FIGURE 1. BETIW - Evolution in space x and time t of the biomass density B illustrated for varying precipitation rates p : (a) 0.7, (b) 1.0, and (c) 2.0, obtained by numerically simulating equations (2) with initial condition (9) considering $T_0 = 0$, $\mathcal{A} = 0.8$ and $k = 0.001$ while the other parameter values are considered as in Table 3.

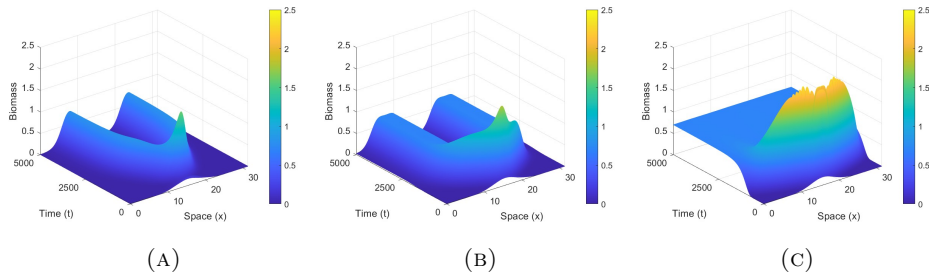


FIGURE 2. BETIW - Evolution in space x and time t of the biomass density B illustrated for varying precipitation rates p : (a) 0.7, (b) 1.0, and (c) 2.0, obtained by numerically simulating equations (2) with initial condition (9) considering $T_0 = 0$, $\mathcal{A} = 0.2$ and $k = 0.001$ while the other parameter values are considered as in Table 3.

availability of biomass, which in our simulations is given by the parameter \mathcal{A} of the initial condition. In particular, in Fig. 1 where \mathcal{A} is higher ($\mathcal{A} = 0.8$), we notice that in two cases we get patterns, while in the case of higher water availability, this leads to a constant steady-state solution. In Fig. 2, where \mathcal{A} is taken as intermediate ($\mathcal{A} = 0.2$), we notice the same behavior asymptotically while there are more oscillations in the transient phase. In Fig. 3, we observe a very different behavior; when \mathcal{A} is taken below a certain threshold ($\mathcal{A} = 0.1$), we observe extinction of the biomass if the precipitation rate is below a critical value. On the other hand, in the third panel of Fig. 3, we observe a constant, non-zero, asymptotic solution (notice that the transient behavior is cropped to maintain the same scale as the other panels in the same figure).

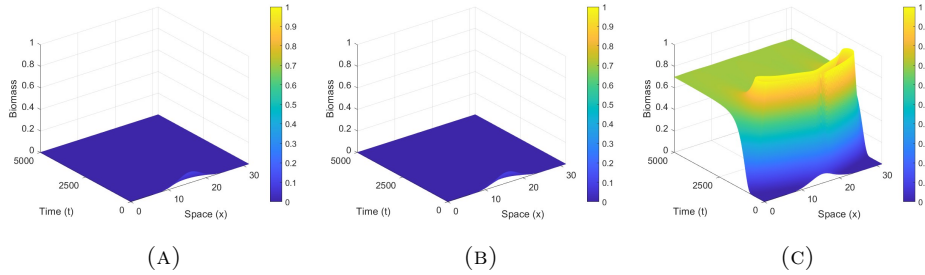


FIGURE 3. BETIW - Evolution in space x and time t of the biomass density B illustrated for varying precipitation rates p : (a) 0.7, (b) 1.0, and (c) 2.0, obtained by numerically simulating equations (2) with initial condition (9) considering $T_0 = 0$, $\mathcal{A} = 0.1$ and $k = 0.001$ while the other parameter values are considered as in Table 3.

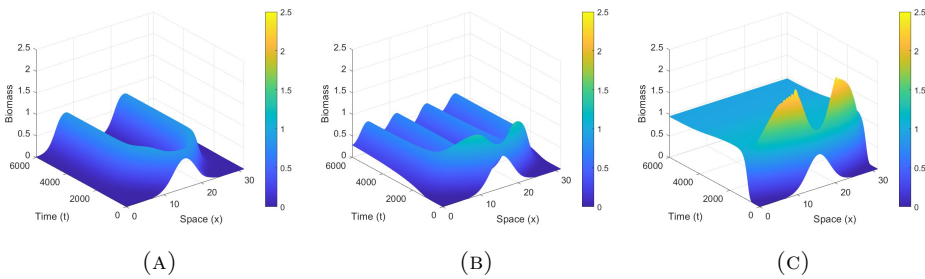


FIGURE 4. BETMW - Evolution in space x and time t of the biomass density B illustrated for varying precipitation rates p : (a) 0.7, (b) 1.0, and (c) 2.0, obtained by numerically simulating equations (3) with initial condition (9) having $T_0 = 0.0001$, $\mathcal{A} = 0.8$ and $k = 0.01$ while the other parameter values are considered as in Table 3.

4.3. **Results for BETMW model.** Regarding the BETMW model (Figures 4-6), the results show that, depending on the precipitation rate and the initial biomass, the model can display patterns or constant steady state behavior for biomass, as in the BETIW model. Specifically, we observe that in Fig. 4, when \mathcal{A} is higher ($\mathcal{A} = 0.8$ or $\mathcal{A} = 0.2$), we have patterns in two cases. However, the BETMW model produces an increasing number of peaks with $p = 1$, in contrast to the BETIW model. On the other hand, this leads to a constant steady state solution when there is more water available ($p = 2$). A similar behavior is observed asymptotically in Fig. 5, where \mathcal{A} is assumed to be intermediate, but with greater oscillations in the transient phase. We observe a significantly different behavior in Fig. 6 when \mathcal{A} is taken below a certain threshold ($\mathcal{A} = 0.1$), if the precipitation rate falls below a critical value, we observe biomass extinction. However, for $p = 2$, a constant, non-zero, asymptotic solution

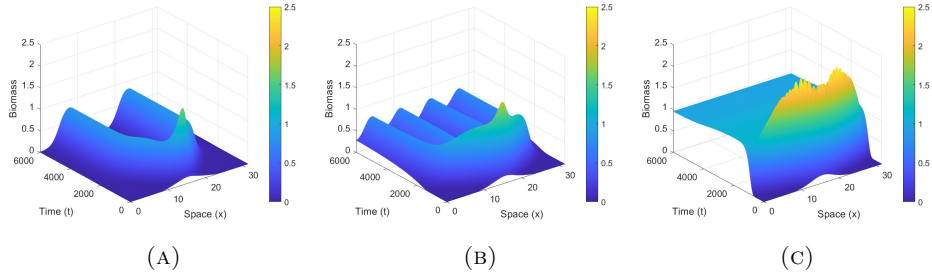


FIGURE 5. BETMW - Evolution in space x and time t of the biomass density B illustrated for varying precipitation rates p : (a) 0.7, (b) 1.0, and (c) 2.0, obtained by numerically simulating equations (3) with initial condition (9) having $T_0 = 0.0001$, $\mathcal{A} = 0.2$ and $k = 0.01$ while the other parameter values are considered as in Table 3.

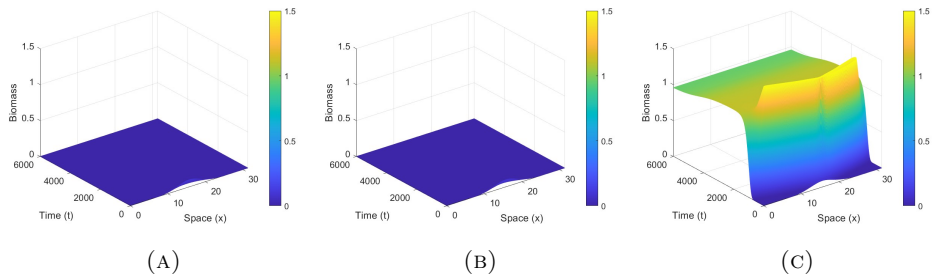


FIGURE 6. BETMW - Evolution in space x and time t of the biomass density B illustrated for varying precipitation rates p : (a) 0.7, (b) 1.0, and (c) 2.0, obtained by numerically simulating equations (3) with initial condition (9) having $T_0 = 0.0001$, $\mathcal{A} = 0.1$ and $k = 0.01$ while the other parameter values are considered as in Table 3.

can be observed in the third panel of Fig. 6 (notice that the transient behavior is cropped to maintain the same scale as the other panels in the same figure).

4.4. Results for BETIMW model. The results for the BETIMW model (Fig. 7-9) are consistent with those of the BETMW model. In particular, we see patterns with the increasing number of peaks (Fig. 7 and 8) with a greater value of p ($p = 1$) and \mathcal{A} ($\mathcal{A} = 0.8$ or $\mathcal{A} = 0.2$). Furthermore, the BETIMW model leads to a constant steady state solution when there is additional water available ($p = 2$). In Fig. 9 when \mathcal{A} is taken below a certain threshold ($\mathcal{A} = 0.1$), biomass extinction occurs if the precipitation rate is below a critical value and a constant, non-zero, asymptotic solution can be observed for $p = 2$. (notice that the transient behavior is cropped to maintain the same scale as the other panels in the same figure).

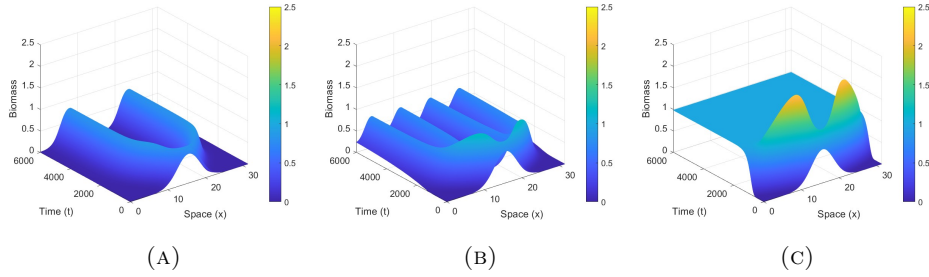


FIGURE 7. BETIMW - Evolution in space x and time t of the biomass density B illustrated for varying precipitation rates p : (a) 0.7, (b) 1.0, and (c) 2.0, obtained by numerically simulating equations (4) with initial condition (9) considering $T_0 = 0$, $\mathcal{A} = 0.8$ and $k = 0.1$ while the other parameter values are considered as in Table 3.

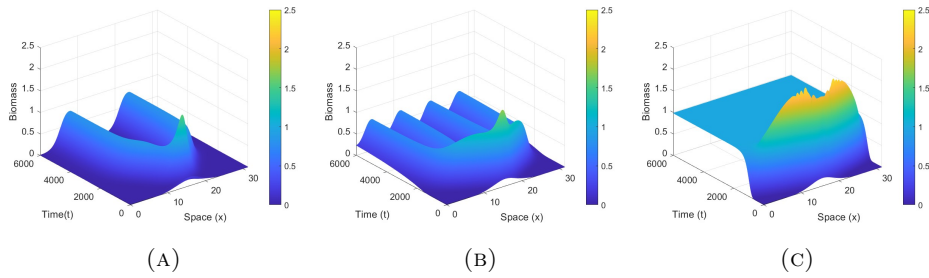


FIGURE 8. BETIMW - Evolution in space x and time t of the biomass density B illustrated for varying precipitation rates p : (a) 0.7, (b) 1.0, and (c) 2.0, obtained by numerically simulating equations (4) with initial condition (9) considering $T_0 = 0$, $\mathcal{A} = 0.2$ and $k = 0.1$ while the other parameter values are considered as in Table 3.

4.5. Results for the models with logistic biomass growth. The results show that in the case of the models with logistic biomass growth (Fig. 10-15) exhibits steady state behavior for biomass for all values of p and \mathcal{A} . For each three models, we observe a comparable steady state in the figure with an associated value of \mathcal{A} , but at a higher uniform biomass level for a higher precipitation value p .

The first difference to note is that the modeled ecological system produces patterns when biomass growth is exponential, whereas, with logistic growth, it always goes to a uniform solution. In ecological terms, this means that if the biomass is limited by other factors (space, nutrients, light, etc.), implicitly described by logistic growth, it manages to arrive at a stable system value without producing patterns in space.

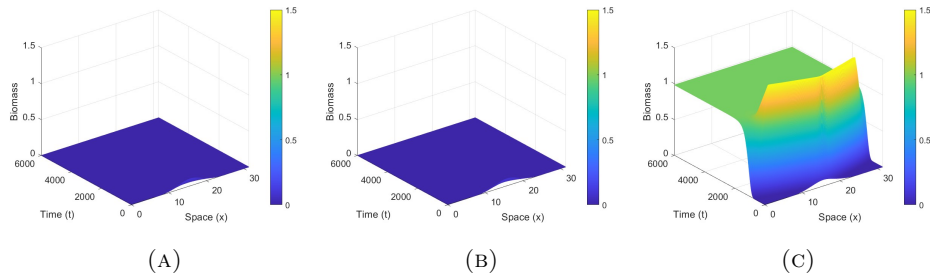


FIGURE 9. BETIMW - Evolution in space x and time t of the biomass density B illustrated for varying precipitation rates p : (a) 0.7, (b) 1.0, and (c) 2.0, obtained by numerically simulating equations (4) with initial condition (9) considering $T_0 = 0$, $\mathcal{A} = 0.1$ and $k = 0.1$ while the other parameter values are considered as in Table 3.

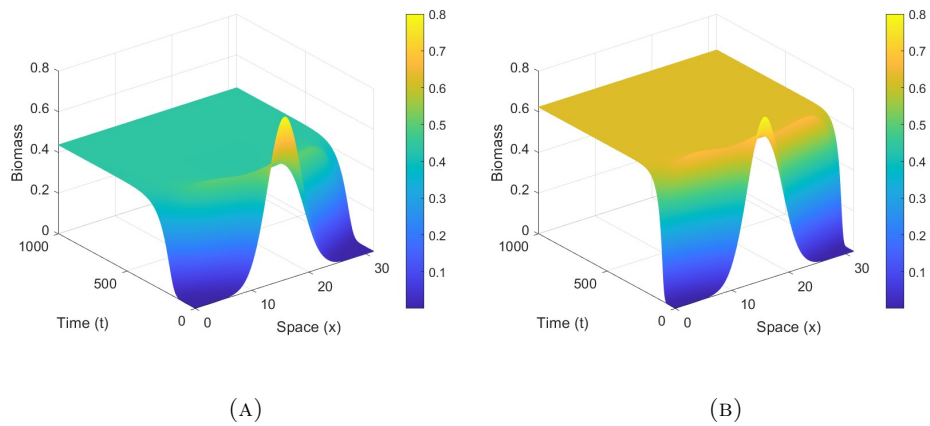


FIGURE 10. BLTIW - Evolution in space x and time t of the biomass density B illustrated for varying precipitation rates p : (a) 0.7, and (b) 2.0, obtained by numerically simulating equations (5) with initial condition (9) considering $T_0 = 0$, $\mathcal{A} = 0.8$ and $k = 0.01$ while the other parameter values are considered as in Table 3.

The introduction of water into the biomass-toxicity dynamics resulted in the BETIW, BETMW, and BETIMW models also producing patterns, in contrast to our previous work [1]. In particular, in the models considered in the present work, the presence of water creates feedback in the biomass-toxicity dynamics leading to the occurrence of Turing conditions with certain parameter sets ($p = 0.7$ and $p = 1.0$) and consequently, the formation of patterns (Fig. 1, 2, 4, 5, 7, 8) whereas in the absence of water in the model the system would go towards infinite biomass growth or uniform biomass regardless of the precipitation value [1].

From the numerical simulations and in the breadth of the domain considered, it can be observed that the BETIW model always produces two peaks under conditions

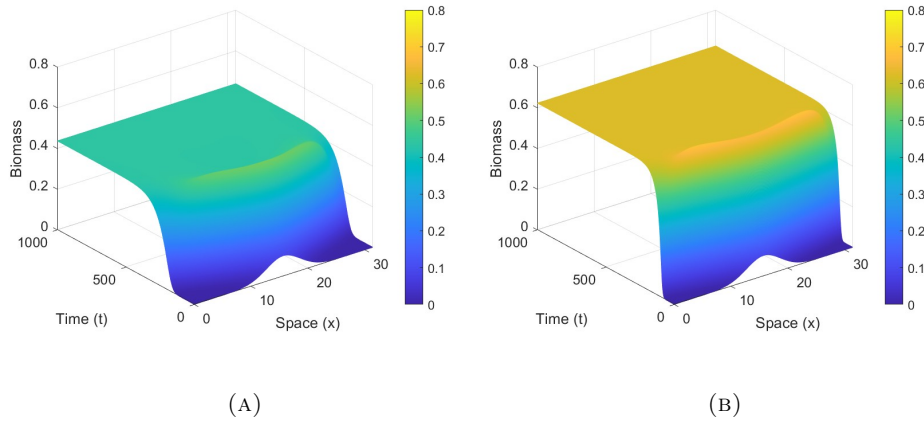


FIGURE 11. BLTIW - Evolution in space x and time t of the biomass density B illustrated for varying precipitation rates p : (a) 0.7, and (b) 2.0, obtained by numerically simulating equations (5) with initial condition (9) considering $T_0 = 0$, $\mathcal{A} = 0.1$ and $k = 0.01$ while the other parameter values are considered as in Table 3.

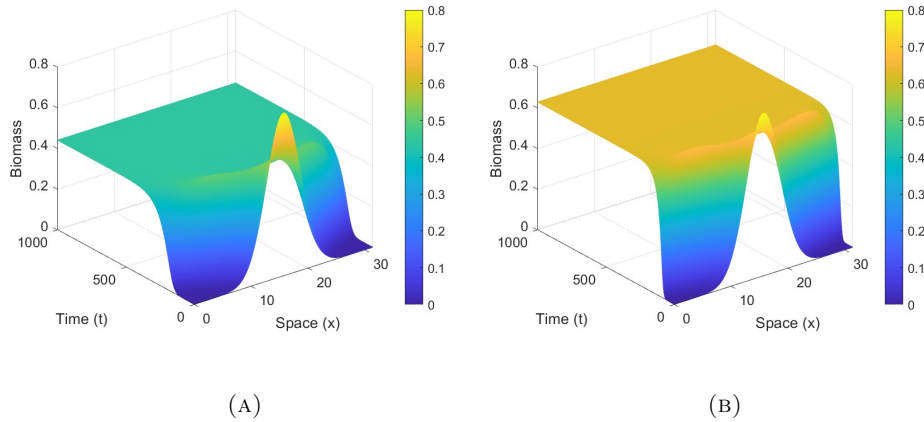


FIGURE 12. BLTMW - Evolution in space x and time t of the biomass density B illustrated for varying precipitation rates p : (a) 0.7, and (b) 2.0, obtained by numerically simulating equations (6) with initial condition (9) considering $T_0 = 0$, $\mathcal{A} = 0.8$ and $k = 0.01$ while the other parameter values are considered as in Table 3.

with a sufficiently large initial biomass value ($\mathcal{A} = 0.8$ or $\mathcal{A} = 0.2$) (Fig. 1 and 2), whereas the BETMW and BETIMW models produce increasing numbers of peaks as the initial biomass increases (Fig. 4, 5 and Fig. 7, 8). In ecological terms, the BETIW system produces two vegetation spots with a larger size (i.e. diameter) than the four vegetation spots with a smaller size in the other two models.

5. Discussion. In this work, we have examined how autotoxicity and water availability contribute to the development of spatial patterns. We have presented a

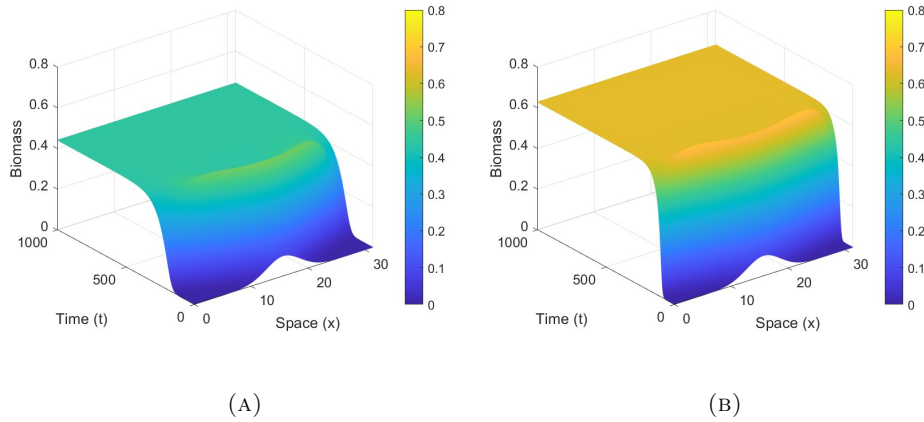


FIGURE 13. BLTMW - Evolution in space x and time t of the biomass density B illustrated for varying precipitation rates p : (a) 0.7, and (b) 2.0, obtained by numerically simulating equations (6) with initial condition (9) considering $T_0 = 0$, $\mathcal{A} = 0.1$ and $k = 0.01$ while the other parameter values are considered as in Table 3.

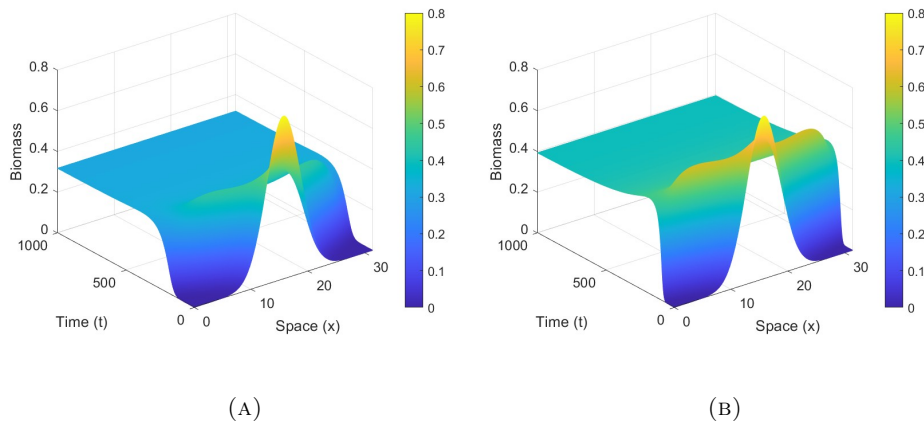


FIGURE 14. BLTIMW - Evolution in space x and time t of the biomass density B illustrated for varying precipitation rates p : (a) 0.7, and (b) 2.0, obtained by numerically simulating equations (7) with initial condition (9) considering $T_0 = 0$, $\mathcal{A} = 0.8$ and $k = 0.01$ while the other parameter values are considered as in Table 3.

comparison between different reaction-diffusion PDE models that explain the dynamics of plant biomass in the presence of toxicity produced by litter decomposition and water scarcity. We included mortality and inhibitor terms in our models to capture the components' individual death rates and inhibitory effects and logistic and exponential growth functions to reflect various growth patterns.

In order to present the complete analysis and forecasting, and to tighten the numerical results obtained with the analysis of stable and unstable branches of

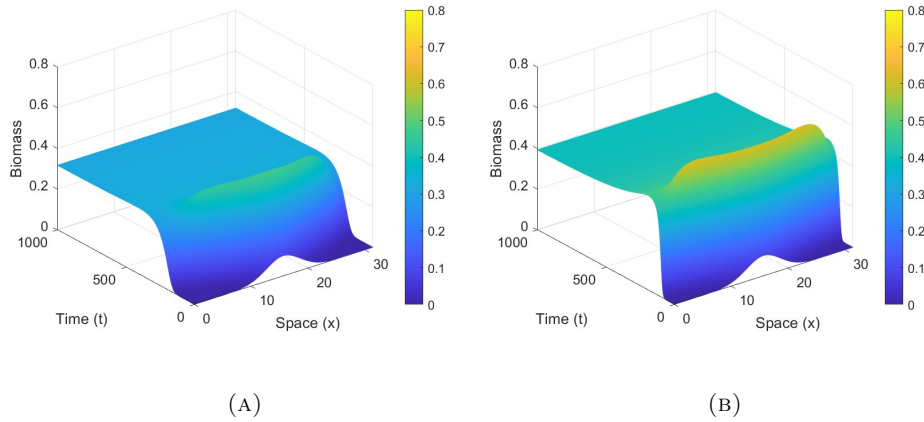


FIGURE 15. BLTIMW - Evolution in space x and time t of the biomass density B illustrated for varying precipitation rates p : (a) 0.7, and (b) 2.0, obtained by numerically simulating equations (7) with initial condition (9) considering $T_0 = 0$, $\mathcal{A} = 0.1$ and $k = 0.01$ while the other parameter values are considered as in Table 3.

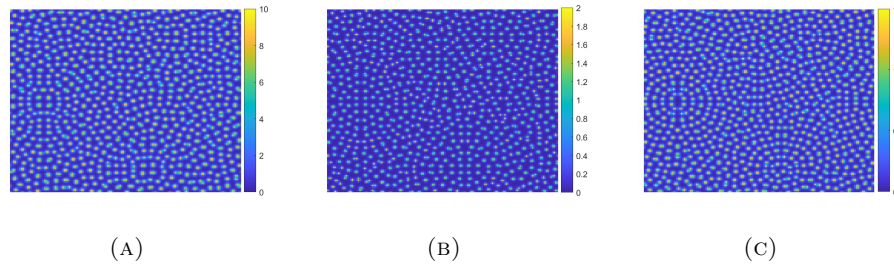


FIGURE 16. Exponential Growth Models - Distribution of the biomass density B in the x - y plane for BETIW, BETMW, and BETIMW models in (a), (b), and (c), obtained by numerically simulating equations (2), (3), and (4) with initial condition (9) considering $T_0 = 0$, $A = 0.6$, $p = 0.7$, and $k = 0.001$, $k = 0.01$, and $k = 0.1$ respectively, while the other parameter values are considered as in Table 3.

solutions, we have focused our numerical investigation on a one-dimensional spatial domain; however, an analogous analysis can be conducted in two dimensions. As an example, we present in Fig. 16, 17 the obtained asymptotic solutions by considering a 2D square domain divided in 150×150 subdomains. Initially, we assume that the biomass is non zero only on four Gaussian peaks (with height $\mathcal{A} = 0.6$ and width $\sigma = 0.3$) distributed randomly in the square domain. We can model the development and dispersal of biomass from discrete seed locations using this initial condition. We consider periodic boundary conditions for the lattice, which essentially wraps around our square domain, removes edge effects. This is a common framework in

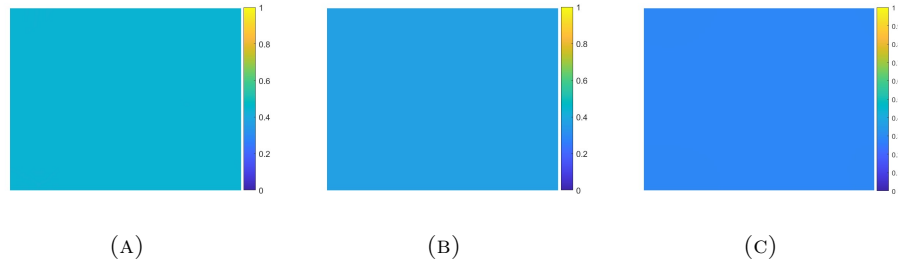


FIGURE 17. Logistic Growth Models - Distribution of the biomass density B in the x - y plane for BLTIW, BLTMW, and BLTIMW models in (a), (b), and (c), obtained by numerically simulating equations (5), (6), and (7) with initial condition (9) considering $T_0 = 0$, $A = 0.6$, $p = 0.7$, and $k = 0.01$, respectively, while the other parameter values are considered as in Table 3.

the present application because replicates a wider, continuous setting well-suited for studying pattern formation and long-range interactions in ecological systems.

As can be observed in Fig. 16, spotted patterns of different heights appear, that are typical of such vegetation behavior, and also some constant biomass behavior can be reached by the different models applied with the same choice of parameters. Notice that in the three cases of exponential models we have chosen different death rates of toxicity so to forecast different scenarios. The wide range of results indicates that these models may prove to be powerful tools for analyzing real landscape conditions that are demonstrated in satellite photography (aerial photographs). Also, the modelling framework presented in this work can provide guidance in the construction of policies against desertification based on the ecological environment. As the six models provided here lead to six different ecological scenarios even though all systems consider the same soil conditions and the same plant species, we can deduce that the growth and inhibition dynamics play an important role in the evolution of the system dynamics.

Through a comparison between the patterns generated by our models and those found in satellite photographs, it could be possible to determine the ecological processes and underlying environmental conditions that are present in a particular terrain. This approach could be useful for determining stress hotspots, forecasting ecosystem health, or comprehending resource distribution in space. From this information, one could deduce which of the six modelling approaches illustrated here should be applied in order to better forecast the future dynamics. This gives that we have a powerful set of choices when modeling what is known for aerial photographs of real vegetation patterns and can apply the best of the six models for forecasting. Thus, our modelling strategies offer a viable way to convert satellite information into insightful ecological assessments that could support conservation initiatives, land management choices, or the early identification of changes in ecosystems. In future work, we intend to enhance our methodology with the help of available satellite data in order to give valuable predictions and indications.

Appendix A. Equilibria and stability. In this section, we outline the steady-states for each of the six models under consideration and perform numerical continuation to investigate their stability, as well as the emergence of bifurcations leading

to patterns. All models admit three equilibria, which we denote as (B_0^*, W_0^*, T_0^*) , (B_+^*, W_+^*, T_+^*) , and (B_-^*, W_-^*, T_-^*) . In all cases, the first steady-state (corresponding to bare soil) is given by

$$(B_0^*, W_0^*, T_0^*) = \left(0, \frac{p}{l}, 0\right). \tag{12}$$

This steady-state is always stable w.r.t. homogeneous perturbations in the case of the BETIW, BETMW, and BETIMW models, whereas it undergoes a Turing bifurcation at $p = \frac{dl}{g}$ in the case of the BLTIW, BLTMW, and BLTIMW models.

The remaining equilibria correspond to uniform vegetation and vary depending on the model considered. The stability of these steady-states is then explored numerically using the software `pde2path` [49] focusing on the 1D case. In particular, we consider a grid of length 30 and fix all parameter values except for the precipitation rate p . The diagrams shown in each section all show on the vertical axis the L_2 -norm of the biomass density, indicated by $\|B\|_2$.

A.1. BETIW model. In this case, the steady-states corresponding to uniform vegetation are given by

$$\begin{aligned} B_{\pm}^* &= \frac{gkp \pm \sqrt{g^2k^2p^2 - 4dkl(cdgp + dkr)}}{2(cdgp + dkr)}, \\ W_{\pm}^* &= \frac{p}{(B_{\pm}^*)^2r + l}, \\ T_{\pm}^* &= 1 - \frac{dr((B_{\pm}^*)^2 + l)}{gpB_{\pm}^*}. \end{aligned} \tag{13}$$

These steady-states are admissible (i.e. all their components are nonnegative) as long as

$$p \geq \frac{cdl + 2d\left(\sqrt{l(c^2d^2l + k^2r)}\right)}{gk}. \tag{14}$$

A.2. BETMW model. In this case, the steady-states corresponding to uniform vegetation are given by

$$\begin{aligned} B_{\pm}^* &= \frac{gkp \pm \sqrt{k(g^2kp^2 - 4dl(cgps + dkr))}}{2(cgps + dkr)}, \\ W_{\pm}^* &= \frac{p}{r(B_{\pm}^*)^2 + l}, \\ T_{\pm}^* &= \frac{cdB_{\pm}^*}{k - csB_{\pm}^*}. \end{aligned} \tag{15}$$

These steady-states are admissible (i.e. all their components are nonnegative) as long as

$$p \geq \frac{cls + 2d\left(\sqrt{l(c^2ls^2 + k^2r)}\right)}{gk}. \tag{16}$$

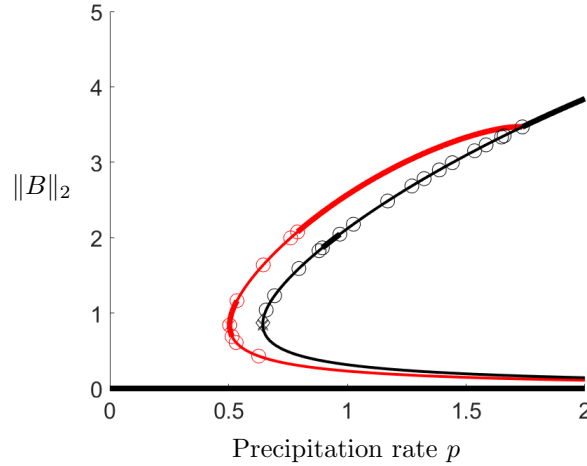


FIGURE 18. Bifurcation diagram obtained with `pde2path` on a 1-dimensional domain of size 30 for the BETIW model. Thick (thin) lines indicate stable (unstable) equilibria. The black curves represent homogeneous steady-states, whereas the red curve represents a branch bifurcating from a selected Turing bifurcation point (indicated by open circles). The parameter values are $D_B = 0.01$, $D_W = 0.8$, $D_T = 0.5$, $g = 0.002$, $d = 0.01$, $r = 0.35$, $l = 0.01$, $c = 0.05$, $k = 0.001$.

A.3. BETIMW model. In this case, the steady-states corresponding to uniform vegetation are given by

$$\begin{aligned} B_{\pm}^* &= \frac{gkp \pm \sqrt{k(k(g^2p^2 - 4d^2lr) - 4dglp(c_1 + c_2)(d + s))}}{2(gp(c_1 + c_2)(d + s) + dkr)}, \\ W_{\pm}^* &= \frac{p}{r(B_{\pm}^*)^2 + l}, \\ T_{\pm}^* &= \frac{gpB_{\pm}^* - d(r(B_{\pm}^*)^2 + l)}{rs(B_{\pm}^*)^2 + gpB_{\pm}^* + ls}. \end{aligned} \quad (17)$$

These steady-states are admissible (i.e. all their components are nonnegative) as long as

$$p \geq \frac{2d \left(\sqrt{l(l(c_1 + c_2)^2(d + s)^2 + k^2r)} + l(c_1 + c_2)(d + s) \right)}{gk}. \quad (18)$$

A.4. BLTIW model. In this case, the steady-states corresponding to uniform vegetation are given by

$$\begin{aligned} B_{\pm}^* &= \frac{B_{\max}cdgp + gkp \pm \sqrt{4B_{\max}dk(dl - gp)(cgp - B_{\max}kr) + (B_{\max}cdgp + gkp)^2}}{2d(cgp - B_{\max}kr)}, \\ W_{\pm}^* &= \frac{p}{(B_{\pm}^*)^2r + l}, \end{aligned}$$

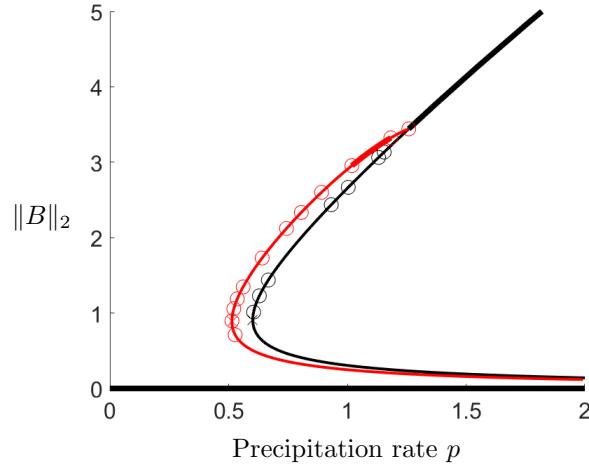


FIGURE 19. Bifurcation diagram obtained with `pde2path` on a 1-dimensional domain of size 30 for the BETMW model. Thick (thin) lines indicate stable (unstable) equilibria. The black curves represent homogeneous steady-states, whereas the red curve represents a branch bifurcating from a selected Turing bifurcation point (indicated by open circles). The parameter values are $D_B = 0.01$, $D_W = 0.8$, $D_T = 0.5$, $g = 0.002$, $d = 0.01$, $r = 0.35$, $l = 0.01$, $c = 0.05$, $k = 0.01$, $s = 0.2$.

$$T_{\pm}^* = \frac{(B_{\pm}^*)^2 B_{\max} dr + B_{\pm}^* gp + B_{\max} dl - B_{\max} gp}{B_{\pm}^* gp - B_{\max} gp}. \tag{19}$$

The equilibrium (B_+^*, W_+^*, T_+^*) is admissible (i.e. all its components are nonnegative) as long as

$$p > \frac{B_{\max} kr}{cg}. \tag{20}$$

On the other hand, the steady-state (B_-^*, W_-^*, T_-^*) is admissible (i.e. all its components are nonnegative) as long as

- $0 < l < \frac{B_{\max} kr}{cs}$ and $\frac{dl}{g} \leq p \neq \frac{B_{\max} dkr}{cgs}$,
- $l = \frac{B_{\max} kr}{cs}$ and $p > \frac{B_{\max} dkr}{cgs}$,
- $l > \frac{B_{\max} kr}{cs}$ and $p \geq \frac{dl}{g}$.

A.5. BLTMW model. In this case, the steady-states corresponding to uniform vegetation are given by

$$B_{\pm}^* = \frac{\pm \sqrt{(B_{\max} c g p s + g k p)^2 - 4 B_{\max} k (d l - g p) (B_{\max} d k r - c g p s)} - g p (B_{\max} c s + k)}{2 (B_{\max} d k r - c g p s)},$$

$$W_{\pm}^* = \frac{p}{r (B_{\pm}^*)^2 + l},$$

$$T_{\pm}^* = \frac{c d B_{\pm}^*}{k - c s B_{\pm}^*}. \tag{21}$$

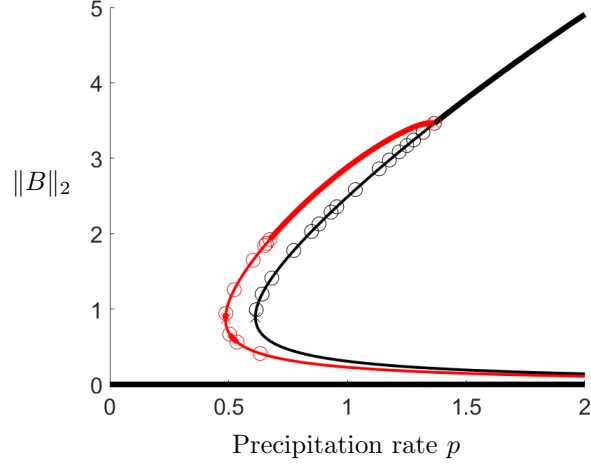


FIGURE 20. Bifurcation diagram obtained with `pde2path` on a 1-dimensional domain of size 30 for the BETIMW model. Thick (thin) lines indicate stable (unstable) equilibria. The black curves represent homogeneous steady-states, whereas the red curve represents a branch bifurcating from a selected Turing bifurcation point (indicated by open circles). The parameter values are $D_B = 0.01$, $D_W = 0.8$, $D_T = 0.5$, $g = 0.002$, $d = 0.01$, $r = 0.35$, $l = 0.01$, $c_1 = c_2 = 0.05$, $k = 0.1$, $s = 0.2$.

However, the equilibrium (B_-^*, W_-^*, T_-^*) is never admissible, since at least one of its component is negative for any choice of parameter values. On the other hand, the steady-state (B_+^*, W_+^*, T_+^*) is admissible as long as

- $0 < l < \frac{B_{\max}kr}{cs}$ and $\frac{dl}{g} \leq p \neq \frac{B_{\max}dkr}{cgs}$,
- $l = \frac{B_{\max}kr}{cs}$ and $p > \frac{B_{\max}dkr}{cgs}$,
- $l > \frac{B_{\max}kr}{cs}$ and $p \geq \frac{dl}{g}$.

A.6. BLTIMW model. In this case, the steady-states corresponding to uniform vegetation are given by

$$\begin{aligned}
 B_{\pm}^* &= \frac{\pm \sqrt{g^2 p^2 (B_{\max}(c_1 + c_2)(d + s) + k)^2 - 4B_{\max}k(dl - gp)(B_{\max}dkr - (c_1 + c_2)gp(d + s))}}{2(B_{\max}dkr - (c_1 + c_2)gp(d + s))} \\
 &\quad + \frac{-B_{\max}gp(c_1 + c_2)(d + s) - gkp}{2(B_{\max}dkr - (c_1 + c_2)gp(d + s))}, \\
 W_{\pm}^* &= \frac{p}{r(B_{\pm}^*)^2 + l}, \\
 T_{\pm}^* &= \frac{B_{\max}gp - B_{\max}d((B_{\pm}^*)^2 r + l) - gpB_{\pm}^*}{(B_{\pm}^*)^2 B_{\max}rs - gpB_{\pm}^* + B_{\max}gp + B_{\max}ls}.
 \end{aligned} \tag{22}$$

The equilibrium (B_-^*, W_-^*, T_-^*) is admissible as long as

$$0 < B_{\max} < \frac{k}{c_1 s + c_2 s} \quad \text{and} \quad p > \frac{B_{\max}kr}{cg}. \tag{23}$$

On the other hand, the existence conditions for the steady-state (B_+, W_+, T_+^*) are quite involved due to the high number of parameters in the model; we therefore omit them for sake of readability. Consistently with the numerical simulations shown in

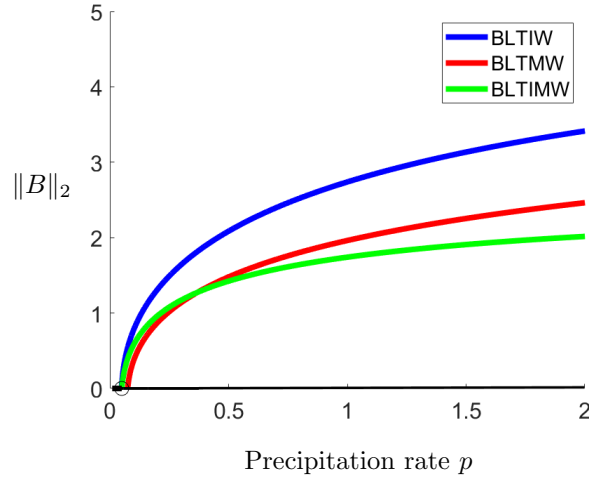


FIGURE 21. Comparison of bifurcation diagrams obtained with `pde2path` on a 1-dimensional domain of size 30. The solid curves correspond to the homogeneous bifurcation branches for the BLTIW (blue), BLTMW (red) and BLTIMW (green) models. In all cases, the homogeneous steady-state remains stable with respect to heterogeneous perturbations, whereas the bare soil steady-state undergoes a bifurcation at $p = \frac{dl}{g}$. The parameter values are $D_B = 0.01$, $D_W = 0.8$, $D_T = 0.5$, $g = 0.002$, $d = 0.01$, $B_m = 1$, $r = 0.35$, $l = 0.01$, $c = 0.05$, $k = 0.01$, $s = 0.2$.

Sec. 4, in all these three cases there are no Turing bifurcation points and no patterns emerge from the homogeneous vegetation branches of equilibria.

Acknowledgments. FG and FC were partially supported by PRIN 2022 PNRR P2022WC2ZZ “A multidisciplinary approach to evaluate ecosystems resilience under climate change”; FG and FC are members of the INdAM research group GNCS and were partially supported by GNCS-INdAM, whereas AI is a member of the INdAM group GNFM; these supports are gratefully acknowledged.

REFERENCES

[1] M. Abbas, F. Giannino, A. Iuorio, Z. Ahmad and F. Calabró, [PDE models for vegetation biomass and autotoxicity](#), *Mathematics and Computers in Simulation*, **228** (2025), 386-401.
 [2] C. K. Augspurger and others, Spatial patterns of damping-off disease during seedling recruitment in tropical forests, *Pests, Pathogens and Plant Communities*, (1990), 131-144.
 [3] R. Bastiaansen, P. Carter and A. Doelman, [Stable planar vegetation stripe patterns on sloped terrain in dryland ecosystems](#), *Nonlinearity*, **32** (2019), 2759-2814.
 [4] G. Bonanomi, G. Incerti, E. Barile, M. Capodilupo, V. Antignani, A. Mingo, V. Lanzotti, F. Scala and S. Mazzoleni, [Phytotoxicity, not nitrogen immobilization, explains plant litter inhibitory effects: Evidence from solid-state \$^{13}C\$ NMR spectroscopy](#), *New Phytologist*, **191** (2011), 1018-1030.

- [5] G. Bonanomi, M. Zotti, M. Idbella, P. Termolino, V. De Micco and S. Mazzoleni, [Field evidence for litter and self-DNA inhibitory effects on *Alnus glutinosa* roots](#), *New Phytologist*, **236** (2022), 399-412.
- [6] F. Borgogno, P. D'Odorico, F. Laio and L. Ridolfi, [Mathematical models of vegetation pattern formation in ecohydrology](#), *Reviews of Geophysics*, **47** (2009), 1.
- [7] G. W. Bruehl and others, *Soilborne Plant Pathogens*, Macmillan Publishing Company, 1987.
- [8] J. J. Burdon, *Diseases and Plant Population Biology*, CUP Archive, 1987.
- [9] S. K. Carter, L. Burris, C. T. Domschke, S. L. Garman, T. Haby, B. R. Harms, E. Kachergis, S. Litschert and K. H. Miller, [Identifying policy-relevant indicators for assessing landscape vegetation patterns to inform planning and management on multiple-use public lands](#), *Environmental Management*, **68** (2021), 426-443.
- [10] G. Consolo and G. Valenti, [Secondary seed dispersal in the Klausmeier model of vegetation for sloped semi-arid environments](#), *Ecological Modelling*, **402** (2019), 66-75.
- [11] E. Constantinescu and D. Deleanu, Diffusion-driven instability in activator-inhibitor model—a mathematical approach to biology.
- [12] H. E. Cosby, Rings on the range, *Rangeland Ecology & Management/Journal of Range Management Archives*, **13** (1960), 283-288.
- [13] J. T. Curtis and G. Cottam, [Antibiotic and autotoxic effects in prairie sunflower](#), *Bulletin of the Torrey Botanical Club*, **77** (1950), 187-191.
- [14] V. Deblauwe, P. Couteron, J. Bogaert and N. Barbier, [Determinants and dynamics of banded vegetation pattern migration in arid climates](#), *Ecological Monographs*, **82** (2012), 3-21.
- [15] L. Eigentler and J. A. Sherratt, [An integrodifference model for vegetation patterns in semi-arid environments with seasonality](#), *Journal of Mathematical Biology*, **81** (2020), 875-904.
- [16] P. Gandhi, L. Werner, S. Iams, K. Gowda and M. Silber, [A topographic mechanism for arcing of dryland vegetation bands](#), *Journal of The Royal Society Interface*, **15** (2018), 20180508.
- [17] E. Gilad, J. von Hardenberg, A. Provenzale, M. Shachak and E. Meron, [Ecosystem engineers: From pattern formation to habitat creation](#), *Physical Review Letters*, **93** (2004), 098105.
- [18] K. Gowda, S. Iams and M. Silber, [Signatures of human impact on self-organized vegetation in the Horn of Africa](#), *Scientific Reports*, **8** (2018), 3622.
- [19] G. Grifò, A. Iuorio and F. Veerman, Far-from-equilibrium travelling pulses in sloped semi-arid environments driven by autotoxicity effects, [arXiv:2405.15602](#), 2024.
- [20] R. HilleRisLambers, M. Rietkerk, F. van den Bosch, H. H. Prins and H. de Kroon, Vegetation pattern formation in semi-arid grazing systems, *Ecology*, **82** (2001), 50-61.
- [21] M. Ishikawa and K. Miyajima, [Analyses of pattern formation processes in stochastic activator-inhibitor systems with saturation in growth domains](#), *Proceedings of the 36th ISCIE International Symposium on Stochastic Systems Theory and its Applications*, **2005**, 38-43.
- [22] S. Jiang, X. Chen, K. Smettem and T. Wang, [Climate and land use influences on changing spatiotemporal patterns of mountain vegetation cover in southwest China](#), *Ecological Indicators*, **121** (2021), 107193.
- [23] F. Khan, M. Abbas, J. E. Mac'ias-D'iaz, M. B. Khan and S. M. Alghamdi, [Computational solution of an acid-mediated tumor-growth radial model under logistic growth regimes for normal and cancer cells](#), *International Journal of Biomathematics*, **16** (2023), 2250084.
- [24] C. A. Klausmeier, [Regular and irregular patterns in semiarid vegetation](#), *Science*, **284** (1999), 1826-1828.
- [25] A. Marasco, F. Giannino and A. Iuorio, [Modelling competitive interactions and plant–soil feedback in vegetation dynamics](#), *Ricerche di Matematica*, **69** (2020), 553-577.
- [26] A. Marasco, A. Iuorio, F. Carteni, G. Bonanomi, F. Giannino and S. Mazzoleni, [Water limitation and negative plant-soil feedback explain vegetation patterns along rainfall gradient](#), *Procedia Environmental Sciences*, **19** (2013), 139-147.
- [27] A. Marasco, A. Iuorio, F. Carteni, G. Bonanomi, D. M. Tartakovsky, S. Mazzoleni and F. Giannino, [Vegetation pattern formation due to interactions between water availability and toxicity in plant–soil feedback](#), *Bulletin of Mathematical Biology*, **76** (2014), 2866-2883.
- [28] R. Martínez-García, C. Cabal, J. M. Calabrese, E. Hernández-García, C. E. Tarnita, C. López and J. A. Bonachela, Integrating theory and experiments to link local mechanisms and ecosystem-level consequences of vegetation patterns in drylands, *Chaos, Solitons & Fractals*, **166** (2023), 112881.
- [29] S. Mazzoleni, G. Bonanomi, F. Giannino, M. Rietkerk, S. Dekker and F. Zucconi, [Is plant biodiversity driven by decomposition processes? An emerging new theory on plant diversity](#), *Community Ecology*, **8** (2007), 103-109.

- [30] E. Meron, [From patterns to function in living systems: Dryland ecosystems as a case study](#), *Annual Review of Condensed Matter Physics*, **9** (2018), 79-103.
- [31] E. Meron, E. Gilad, J. Von Hardenberg, M. Shachak and Y. Zarmi, [Vegetation patterns along a rainfall gradient](#), *Chaos, Solitons & Fractals*, **19** (2004), 367-376.
- [32] E. Meron, H. Yizhaq and E. Gilad, [Localized structures in dryland vegetation: Forms and functions](#), *Chaos: An Interdisciplinary Journal of Nonlinear Science*, **17** (2007), 037109.
- [33] J. Nathan, J. von Hardenberg and E. Meron, [Spatial instabilities untie the exclusion-principle constraint on species coexistence](#), *Journal of Theoretical Biology*, **335** (2013), 198-204.
- [34] S. Páez-Bimos, A. Molina, M. Calispa, P. Delmelle, B. Lahuate, M. Villacís, T. Muñoz and V. Vanacker, [Soil-vegetation-water interactions controlling solute flow and transport in volcanic ash soils of the high Andes](#), *Hydrology and Earth System Sciences Discussions*, **2022**, 1-37.
- [35] M. J. Piotrowska, [Activator-inhibitor system with delay and pattern formation](#), *Mathematical and Computer Modelling*, **42** (2005), 123-131.
- [36] M. Rietkerk, M. C. Boerlijst, F. van Langevelde, R. HilleRisLambers, J. van de Koppel, L. Kumar, H. H. T. Prins and A. M. de Roos, [Self-organization of vegetation in arid ecosystems](#), *The American Naturalist*, **160** (2002), 524-530.
- [37] M. Rietkerk and J. V. de Koppel, [Regular pattern formation in real ecosystems](#), *Trends in Ecology & Evolution*, **23** (2008), 169-175.
- [38] M. Rietkerk, P. Ketner, J. Burger, B. Hoorens and H. Olf, [Multiscale soil and vegetation patchiness along a gradient of herbivore impact in a semi-arid grazing system in West Africa](#), *Plant Ecology*, **148** (2000), 207-224.
- [39] P. Saco, G. Willgoose and G. Hancock, [Eco-geomorphology of banded vegetation patterns in arid and semi-arid regions](#), *Hydrology and Earth System Sciences*, **11** (2007), 1717-1730.
- [40] G. Severino, F. Giannino, F. Carteni, S. Mazzoleni and D. M. Tartakovsky, [Effects of hydraulic soil properties on vegetation pattern formation in sloping landscapes](#), *Bulletin of Mathematical Biology*, **79** (2017), 2773-2784.
- [41] J. A. Sherratt, [Pattern solutions of the Klausmeier model for banded vegetation in semiarid environments V: The transition from patterns to desert](#), *SIAM Journal on Applied Mathematics*, **73** (2013), 1347-1367.
- [42] J. A. Sherratt, [An analysis of vegetation stripe formation in semi-arid landscapes](#), *Journal of Mathematical Biology*, **51** (2005), 183-197.
- [43] J. A. Sherratt and A. D. Synodinos, [Vegetation patterns and desertification waves in semi-arid environments: Mathematical models based on local facilitation in plants](#), *Discrete Contin. Dyn. Syst. Ser. B*, **17** (2012), 2815-2827.
- [44] K. Siteur, E. Siero, M. B. Eppinga, J. D. Rademacher, A. Doelman and M. Rietkerk, [Beyond Turing: The response of patterned ecosystems to environmental change](#), *Ecological Complexity*, **20** (2014), 81-96.
- [45] G. Sun, H. Zhang, J. Wang, J. Li, Y. Wang, L. Li, Y. Wu, G. Feng and Z. Jin, [Mathematical modeling and mechanisms of pattern formation in ecological systems: A review](#), *Nonlinear Dynamics*, **104** (2021), 1677-1696.
- [46] S. E. Thompson, S. Assouline, L. Chen, A. Trahtenbrot, T. Svoray and G. G. Katul, [Secondary dispersal driven by overland flow in drylands: Review and mechanistic model development](#), *Movement Ecology*, **2** (2014), 1-13.
- [47] S. Thompson, G. Katul and S. M. McMahon, [Role of biomass spread in vegetation pattern formation within arid ecosystems](#), *Water Resources Research*, **44** (2008), 10.
- [48] A. M. Turing, [The chemical basis of morphogenesis](#), *Bulletin of Mathematical Biology*, **52** (1990), 153-197.
- [49] H. Uecker, D. Wetzell and J. D. M. Rademacher, [pde2path-A Matlab package for continuation and bifurcation in 2D elliptic systems](#), *Numerical Mathematics: Theory, Methods and Applications*, **7** (2014), 58-106.
- [50] N. Ursino and S. Contarini, [Stability of banded vegetation patterns under seasonal rainfall and limited soil moisture storage capacity](#), *Advances in Water Resources*, **29** (2006), 1556-1564.
- [51] N. Ursino and M. C. Rulli, [Combined effect of fire and water scarcity on vegetation patterns in arid lands](#), *Ecological Modelling*, **221** (2010), 2353-2362.
- [52] S. van der Stelt, A. Doelman, G. Hek and J. D. Rademacher, [Rise and fall of periodic patterns for a generalized Klausmeier–Gray–Scott model](#), *Journal of Nonlinear Science*, **23** (2013), 39-95.
- [53] J. von Hardenberg, E. Meron, M. Shachak and Y. Zarmi, [Diversity of vegetation patterns and desertification](#), *Physical Review Letters*, **87** (2001), 198101.

- [54] A. S. Watt, [Pattern and process in the plant community](#), *Journal of Ecology*, **35** (1947), 1-22.
- [55] Y. R. Zelnik, H. Uecker, U. Feudel and E. Meron, [Desertification by front propagation](#), *Journal of Theoretical Biology*, **418** (2017), 27-35.

Received October 2024; revised December 2024; early access December 2024.